A high resolution and high contrast MRI for differentiation of subcortical structures for DBS targeting: The Fast Gray Matter Acquisition T1 Inversion Recovery (FGATIR)

Atchar Sudhyadhom [a,*], Ihtsham U. Haq [b], Kelly D. Foote [a], Michael S. Okun [b], Frank J. Bova [a]

[a] *Department of Neurosurgery, University of Florida, Gainesville, FL, USA*
[b] *Department of Neurology, University of Florida, Gainesville, FL, USA*

ABSTRACT

DBS depends on precise placement of the stimulating electrode into an appropriate target region. Image-based (direct) targeting has been limited by the ability of current technology to visualize DBS targets. We have recently developed and employed a Fast Gray Matter Acquisition T1 Inversion Recovery (FGATIR) 3T MRI sequence to more reliably visualize these structures. The FGATIR provides significantly better high resolution thin (1 mm) slice visualization of DBS targets than does either standard 3T T1 or T2-weighted imaging. The T1 subcortical image revealed relatively poor contrast among the targets for DBS, though the sequence did allow localization of striatum and thalamus. T2 FLAIR scans demonstrated better contrast between the STN, SNr, red nucleus (RN), and pallidum (GPe/GPi). The FGATIR scans allowed for localization of the thalamus, striatum, GPe/GPi, RN, and SNr and displayed sharper delineation of these structures. The FGATIR also revealed features not visible on other scan types: the internal lamina of the GPi, fiber bundles from the internal capsule piercing the striatum, and the boundaries of the STN. We hope that use of the FGATIR to aid initial targeting will translate in future studies to faster and more accurate procedures with consequent improvements in clinical outcomes.

© 2009 Elsevier Inc. All rights reserved.

Background

Deep brain stimulation (DBS) has become an accepted treatment for medication refractory movement disorders (DBSPDSG, 2001; Hung et al., 2007; Wider et al., 2008; Zorzi et al., 2005) and has also been employed for neuropsychiatric indications in several recent trials (Cosyns et al., 2003; Greenberg et al., 2006; Lozano et al., 2008; Temel and Visser-Vandewalle, 2004). The procedure consists of placing a stimulating electrode into a specific brain structure with the intent of locally modulating a basal ganglia circuit consequently improving clinical symptoms. The target chosen depends on the disorder being addressed and on the patient's symptoms. Common targets have included the subthalamic nucleus (STN) (Wider et al., 2008), globus pallidus interna (GPi) (Hung et al., 2007), nucleus accumbens (NAc) and anterior limb of the internal capsule (ALIC) (Nuttin et al., 2003; Okun et al., 2007), cingulate cortex (area 25) (Lozano et al., 2008), and multiple thalamic subregions (Kumar et al., 2003; Pahwa et al., 2006).

The stimulating electrode must be accurately placed within the target region for maximal efficacy (Chen et al., 2006; Amirnovin et al., 2006). Unfortunately, it has proven difficult to image DBS targets precisely enough to allow placement on the basis of stereotactic imaging alone. A number of ancillary methodologies have therefore been employed to improve the accuracy of electrode placement, including intraoperative microelectrode recording (MER), atlas-based mapping, and computer modeling (Chakravarty et al., 2008). These techniques are limited by their dependence on operator experience and by the variation in brain anatomy between patients (Bootin, 2006; Chen et al., 2006; Duffner et al., 2002; Lee et al., 2005; Rampini et al., 2003).

Both T1 and T2 weighted MRI have commonly been employed as adjuncts to stereotactic targeting. Previous groups have typically employed 2D fast spin echo (FSE) sequences to create these T2-weighted images. This method has significantly limited the ability of the operator to acquire small slice thickness images due to gradient hardware requirements. As a compromise many DBS groups acquire thick slice images from multiple orientations (Dormont et al., 2004; Kitajima et al., 2008; Reich et al., 2000; Slavin et al., 2006). T1-weighted imaging in the form of inversion recovery based 2D FSE sequences have also been used to delineate GPi (Pinsker et al., 2008; Reich et al., 2000) and thalamus (Deoni et al., 2005; Mercado et al., 2006), but these methods have been hampered by the need for very thick slices or for longer scan times as well. Currently available clinical protocols do not produce both sufficient image contrast and resolution for DBS targeting based on MRI alone.

We recently employed a 3T MRI sequence that improves upon standard high resolution 3T T1 and T2 protocols. This new approach, which will be referred to in this paper as the Fast Grey Matter

* Corresponding author.
 E-mail address: atchars@neurosurgery.ufl.edu (A. Sudhyadhom).

Acquisition T1 Inversion Recovery (FGATIR), seems in this pilot study to provide improved, high resolution single-millimeter slice visualization of target structures with heightened grey/white matter contrast in regions of interest.

Materials and methods

Subjects

For this pilot study we examined the preoperative scans of three patients with advanced and medication refractory Parkinson's disease ($n = 2$) or essential tremor ($n = 1$) who were to undergo DBS. These patients underwent formal evaluations by a fellowship-trained Movement Disorders Neurologist, a Neurosurgeon, a Psychiatrist, and a Neuropsychologist in order to ensure accuracy of diagnosis by clinical criteria (Okun et al., 2004) as well as absence of significant cognitive or psychiatric comorbidity. Prior to implantation, patients with PD were also required to demonstrate at least a 30% improvement in the motor subsection of the Unified Parkinson's Disease Rating Scale (UPDRS III) between the on and off medication states (Okun et al., 2004).

Preoperative imaging

Each included patient received four scans on the day prior to surgery: a three plane localizing scout, a T1-weighted 3D Magnetization Prepared-Rapid Acquisition Gradient Echo (MP-RAGE), a 3D T2-weighted Fluid Attenuated Inversion Recovery (FLAIR), and a T1-weighted 3D FGATIR (the last three scans were each single volume whole brain scans). All scans were acquired on a clinical Siemens Allegra 3T MRI using a quadrature birdcage headcoil. The total scanning time for all four scans was 30 min. Specific parameters utilized are listed in Table 1.

The FGATIR protocol was developed from a standard MP-RAGE sequence by modifying the inversion pre-pulse from a 90° saturation pulse to a full 180° inversion pulse, allowing for magnetization to become negative and consequently increasing the possible T1 contrast range. The inversion time (TI) was set to ~400 ms in order to nullify the white matter signal. The use of a short inversion time led to the contrast inversion of some regions relative to standard T1; for example, normally dark cerebrospinal fluid (CSF) signal was bright. The echo time (TE) and other parameters were set such that the TI was the dominant weighting factor in the contrast.

Surgical procedure

On the morning of the operation, a Cosman–Roberts–Wells (CRW) head ring was applied under local anesthesia and a high resolution stereotactic head computed tomography (CT) scan was performed. The CT and MRI images were fused using in-house computer software, a software package that is analogous to the Varian™ (Palo Alto, CA) system but with several added features, that facilitated targeting in

"atlas space" by coregistering anatomical landmarks. A Cartesian coordinate system confirmed the patient's mid-commissural point and this point was used as a reference to confirm the target (Okun et al., 2007).

The software utilized allowed the display and registration of a deformable 3D atlas, based on the Schaltenbrand and Bailey (1959) stereotactic atlas which was then overlaid onto the MRI scans. The atlas and scans were used together to target the structure of interest. We employed a two step targeting process. An initial estimate based on anatomic (AC/PC/midline point) coordinates was then followed by direct targeting adjustments using a deformed atlas overlay over image slices as well as direct visualization of target structures. Target selection depended on the underlying disease. Patients with ET had the anterior boundary of the ventralis caudalis nucleus (Vc) of the thalamus targeted. This boundary was estimated based on indirect targeting and confirmed by the use of microelectrode recording (MER, detailed below). The final electrode location was 2 mm anterior to this point along the anterior boundary of the ventral intermediate nucleus of the thalamus (Vim) and the ventralis oralis posterior (Vop) nucleus. Those patients with PD had their initial target points within the motor (dorsolateral) STN or the motor (posterolateral) GPi. The indirect atlas coordinate for the STN target (tip of lead) for an initial MER pass was approximately AP −3 mm, LT 11 mm, and AX −7 mm. The indirect atlas coordinate used for the GPi target for an initial MER pass was approximately AP 1 mm, LT 21 mm, and AX −6 mm. Coordinates were modified from this indirect targeting by using atlas deformation and direct visualization of target structures.

Microelectrode recording and registration

The target coordinates were verified to be within the region of interest via multiple MER passes. Our technique used a 3-D mapping procedure to guide electrode placement. For each pass cellular activity was recorded at millimeter intervals beginning at 30 mm above the selected target and at submillimeter intervals as the microelectrode approached the target region. At each interval the encountered region was determined by the recording neurologist based on the sound and appearance of the recording and the depth at which it was observed. Each such determination was represented in realtime as a color-coded point overlaid on an individual patient's MRI at the corresponding stereotactic coordinates. In addition to single cell recordings, cellular firing in response to passive motion and sensory stimulation was used to delineate the somatotopic organization of the target structure.

The use of registration software allowed the translation of MER passes into a linear map of structure and somatotopy that was then overlaid on a patient's MRI (as in Figs. 2D, 3D, and 4D). A final decision, based on this aggregate map, was then made as to the optimal location to place the permanent DBS electrode. The procedure decision-making process took into account both electrode tip location within the target region and the electrode's proximity to regions near the target that might result in side effects when stimulated.

The precise mapping process used varied by target. For the three targets (STN, GPi, and Vim) we employed a 'true mapping' strategy: we performed a single MER pass and used its results to determine the location of our next MER track. We typically performed three to five passes to confirm a target's boundaries.

For the STN and GPi, we first mapped the anterior–posterior plane intratarget somatotopic extremity and face responses. We next located the boundary between the target structure and the internal capsule. This boundary was marked by a transition from the typical firing pattern of the target structure to the relative silence of the internal capsule. We then confirmed the lateral border of each structure (again by noting the MER transition from cellularity to relative silence). The inferior boundary was recorded near the termination of each MER track — it was defined by the transition to the tonic firing of SNr for the STN or, in the case of the GPi, the

Table 1
Parameters used for the scans in this study: T1-w MP-RAGE, T2-w FLAIR, and T1-w FGATIR.

	T1-w 3D MP-RAGE	T2-w 3D FLAIR	T1-w 3D FGATIR
Repetition time (TR)	1600 ms	6000 ms	3000 ms
Echo time (TE)	4.38 ms	353 ms	4.39 ms
Inversion time (TI)	800 ms	2200 ms	409 ms
Inversion pulse angle	90°	180°	180°
Matrix	384×288	256×240	320×256
Field of view (mm)	256×192	256×240	256×192
Slices	160×1 mm	160×1 mm	160×1 mm
Orientation	Axial	Sagittal	Axial
Bandwidth	130 Hz/Px	1302 Hz/Px	130 Hz/Px
Acquisition time	6:45 min	12:08 min	11:14 min

transition to the light-sensitive activation of the fibers of the optic tract. For the STN we implanted 3 to 3.5 mm posterior to the anterior border and 2.5 to 3 mm medial to the internal capsule boundary with the deepest electrode contact placed at the STN/SNr boundary. For GPi we typically implanted 2.5 to 3 mm anterior to the posterior border (internal capsule) and 2 to 3 mm from the lateral border (GPe) with the deepest electrode contact placed immediately superior to the optic tract.

In the case of Vim implantation the electrode was inserted at a slightly shallower angle than that of the plane of the typical Vc/Vim boundary. This allowed us to locate the anterior border of Vc as we pass through the Vim side of the Vc/Vim border superiorly and the Vc side of that border inferiorly. The transition from Vim to Vc was appreciated as a change from motor-responsive to sensory-responsive cells. We typically implanted the stimulating electrode 2 mm anterior to the hand region of Vc.

Atlas creation and deformation

The atlas used in this work is an in-house created atlas that is based on the sagittal series contours of the Schaltenbrand–Bailey atlas (Schaltenbrand and Bailey, 1959) of subcortical structures. Contours for each of these subcortical structures were created by approximating connections between sagittal Schaltenbrand–Bailey atlas contours using Delaunay triangulation. By applying this algorithm across all sagittal contours, a linear surface with rough edges was produced which fitted points from one contour to corresponding points along neighboring contours. In order to provide a more continuous surface each of these structures was voxelized to a grid of $0.25 \times 0.25 \times 0.25$ mm^3. These structures were then smoothed using a Gaussian filter of full-width half maximum

of 0.5 mm. This process reduced the discontinuities and abnormalities seen with the Schaltenbrand–Bailey atlas but still held relatively true to the original atlas contours. The final result was a smooth surface that approximately matched the size, shape, and location of the original Schaltenbrand–Bailey atlas contours. This digital atlas itself was manually validated against the original Schaltenbrand–Bailey atlas contours by overlaying the former's contours over the corresponding Schaltenbrand–Bailey atlas planes.

The resulting digital atlas can be displayed and deformed to match the anatomy of each particular patient using nine linear degrees of freedom: scaling, translation, and rotation in the medial–lateral, anterior–posterior, and superior–inferior axes. The general procedure for atlas alignment was 1) designation of an anterior/posterior commissure coordinate system (the coordinate system by which the atlas was created in), 2) linear affine transformation of the atlas to a visually determined "best fit" to the patient's anatomy, and 3) further fine adjustments of the atlas to best fit the patient's anatomy to the target region using nearby structures as reference points.

In the case of the thalamus the boundaries are generally visible and can be used to make fine adjustments. For the STN, both the thalamus and substantia nigra boundaries (superior and inferior) can be used to make final adjustments. For the GPi, the medial boundary of striatum and the anterior boundary of the anterior limb of the internal capsule are used for validation. Each of these methods may be utilized with any of the three types of images examined in this paper. Direct visualization of additional structures can be used to aid in the deformation in the cases of FLAIR and FGATIR imaging.

We used two methods to evaluate the deformation accuracy. First, a movement disorders trained neurosurgeon verified that atlas structures neighboring the target region were aligned with imaging data. This neurosurgeon (who has performed approximately 500 DBS
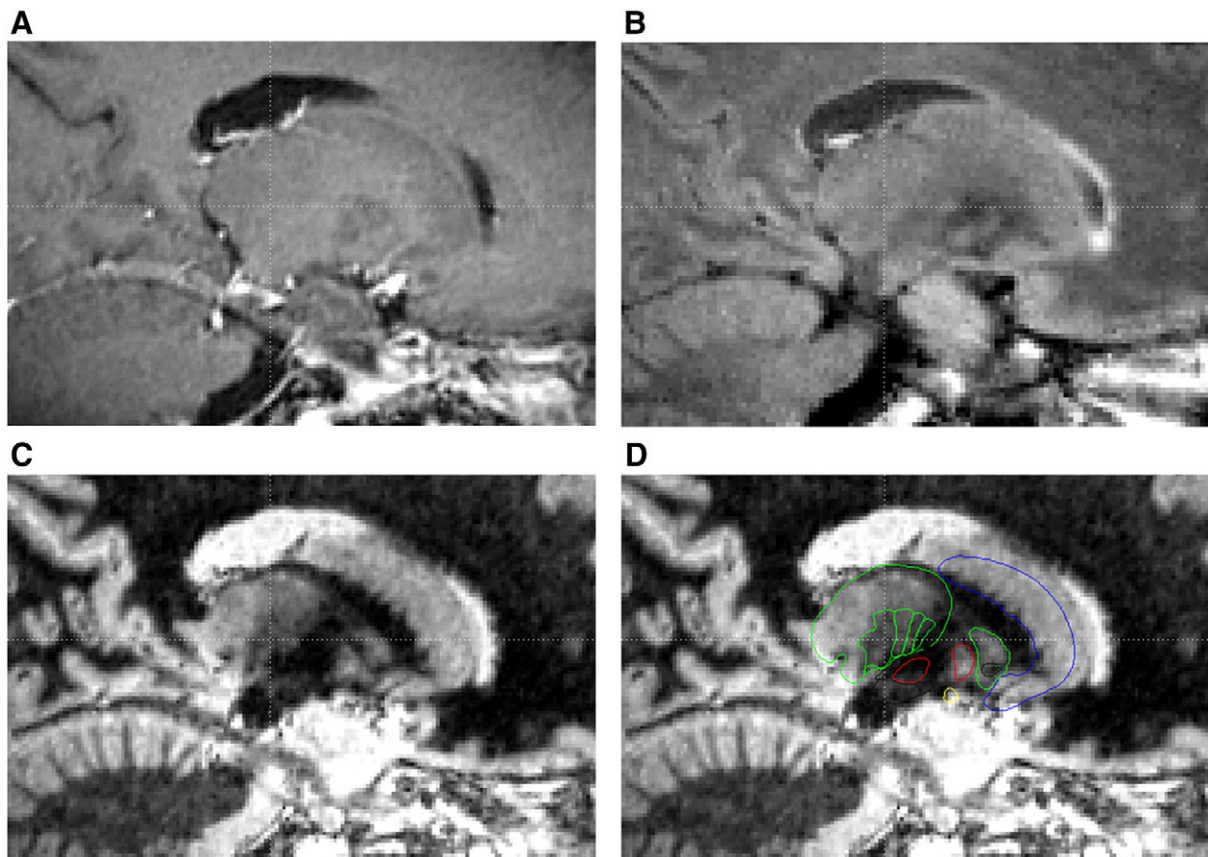

Fig. 1. Sagittal images of subcortical structures in the (A) T1-w 3D MP-RAGE, (B) T2-w 3D FLAIR, (C) T1-w FGATIR, and (D) T1-w FGATIR with deformable atlas contours overlaid. The contour colors for the deformable atlas are (from most anterior to most posterior): striatum (blue), GPe (green), anterior commissure (black), GPi (red), optic tract (yellow), thalamus (green), various VL thalamic nuclei (green), STN (red), and SNr (black).

cases) completed the atlas deformation in all cases to match the patient anatomy with the MR imaging. All images (MP-RAGE/FLAIR/FGATIR) were fused together to provide a complete set of data by which to complete the deformation. An AC/PC coordinate system was chosen for each patient which the atlas was then registered to, so that adjustments were made only after the atlas and patient anatomy were framed within the same coordinate system for all three (mutually fused) image sets.

Second, MER maps were used to physiologically validate correlation between atlas and actual structures lying along the MER path. Intraoperative MER data for the patients in this study showed good correspondence to atlas ROI locations (as seen in Figs. 2D, 3D, and 4D), suggesting that the atlas is a reasonable fit around the targets of interest. We have validated the atlas with microelectrode recording from over 200 patients.

Using both an expert's evaluation and MER data confirmation allowed us to increase our confidence that the atlas deformation chosen provided a robust fit to the structures around the targets.

Analysis

The T1-weighted, T2-weighted FLAIR, and FGATIR sequences were fused to ensure anatomical and stereotactic co-localization. Software was then utilized for the linear affine transformation of the 3D atlas to fit the patient's anatomy (as was described previously). The atlas was then used to delineate structures of interest for qualitative and quantitative analysis. We qualitatively compared our ability to delineate boundaries for the regions of interest among the scan types employed, and quantitatively evaluated the contrast to noise ratio and contrast ratio between areas believed to be within regions of interest and the surrounding area. MER data was used to electrophysiologically verify the boundaries of structures of interest.

For this quantitative analysis the ROI for ventral lateral (VL) thalamus, STN, and GPi were created by using the results of the registration of the deformable atlas. In the case of the VL thalamus, contrast ratios were calculated between the VL thalamus and the non-VL thalamus, as well as between the VL thalamus and the posterior limb of the internal capsule (PLIC). For the STN, contrast ratios were calculated between the STN and the substantia nigra reticulata (SNr) as well as between the STN and the thalamus and finally between STN and ZI. For the GPi, contrast ratios were calculated between the GPi and the PLIC. These ratios are summarized in Fig. 5. The formulas used for contrast to noise ratio and contrast ratio are defined as the following:

Contrast to Noise Ratio (CNR): $|(S_A - S_B)|/($Standard deviation of background noise$)$
Contrast Ratio (CR): $|(S_A - S_B)|/(S_A)$

S_A and S_B are average intensity values for regions A and B, respectively, as determined from ROI created from atlas delineated regions. A set of the voxels outside the patient's head were taken to sample the background noise and this region was used to determine the standard deviation of background noise used in the CNR calculation. The quantitative measure of contrast to noise ratio provides an estimate of the contrast expected between two regions
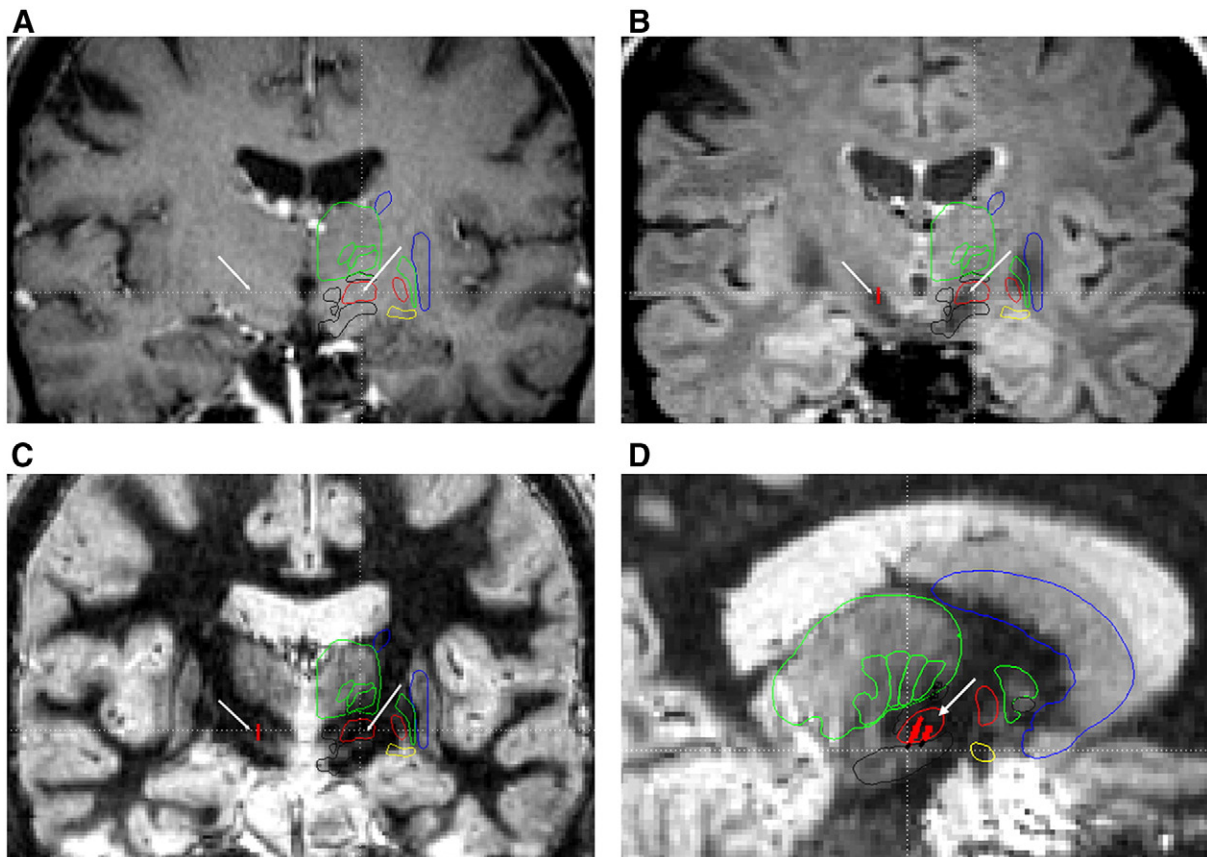

Fig. 2. Subcortical images from a STN DBS patient (pre-surgery) showing coronal slices with deformable atlas contour overlay on the (A) T1-w 3D MP-RAGE, (B) T2-w 3D FLAIR, (C) T1-w FGATIR, and a sagittal slice through the (D) T1-w FGATIR with MER maps overlaid (represented by colored dots). The white arrows represent the location of STN in the coronal and sagittal slices. The red lines in panels B and C (both are the same length) represent the distance (superior to inferior) of the STN in both FLAIR and FGATIR images. Although STN may appear thinner in the FGATIR, as can be seen from the line it is roughly the same size in FLAIR and FGATIR images. In panel D, the dot colors represent cells found for STN (red), thalamus (green), ZI (black and labeled as ZI), and SNr (black and unlabeled). Squares represent regions at which cellular response was seen during either passive movement or sensory stimulation of the patient.

versus the background noise (which would be expected to inhibit contrast difference detection). The contrast ratio (CR) is a more direct measure of contrast but does not take into account noise present within the scan. Since noise characteristics can be improved by changes in hardware or by performing multiple signal averages, both metrics allow us to not only compare the scans as they are but also how noise reduction may improve detecting contrast differences.

Results

Qualitative analysis

The T1-w MP-RAGE subcortical image revealed relatively poor contrast among the targets for DBS, however the sequence did allow reasonable localization of striatum and thalamus. T2-w FLAIR scans demonstrated better contrast and were better able to localize the STN, SNr, red nucleus (RN), and pallidum (GPe/GPi). The FGATIR scans allowed for localization of the thalamus, striatum, GPe/GPi, RN, and SNr and displayed sharper delineation of these structures (Fig. 1). The FGATIR revealed features not visible on other scan types: the internal lamina of the GPi (Fig. 4C, arrow), fiber bundles from the internal capsule piercing the striatum, and the boundaries of the STN.

The T2-w FLAIR sequences poorly imaged the lateral border of STN. Both the FGATIR and T2-w FLAIR (Fig. 2C) displayed the STN as a hypointense structure. However, SNr was hyperintense in the T1-w FGATIR which created a degree of STN/SNR contrast not seen in the T2-w FLAIR. SNr was better visualized by FGATIR than by T2-w FLAIR, and was shown as a hyperintense region inferior to the STN (Figs. 2C,

D). On FGATIR imaging, the lateral and posterior boundaries of STN were also more distinctly hypointense as compared to their appearance on T2-w FLAIR (Figs. 2C,D) which appeared to under-predict the boundaries of STN (according to atlas boundaries). While the lateral boundary is more consistently hypointense on the FGATIR, the definition between the STN and the PLIC was more difficult to visualize than in the T2-w FLAIR. Intraoperative MER mapping confirmed the region of hypointensity that corresponded electro-physiologically to STN.

The FGATIR also produced higher contrast along the lateral boundary of the thalamus than was seen on T2-w FLAIR or standard T1-w scans. We feel it to also be significant that the VL thalamus could be partially distinguished from other thalamic nuclei on FGATIR scans (Fig. 3C). MER data was consistent with the thalamic boundaries seen with FGATIR both spatially and with respect to sensorimotor somatotopy.

The pallidum was hyperintense relative to the posterior limb of the internal capsule (PLIC) on FGATIR imaging. Though both the GPi and striatum were hyperintense they were readily distinguishable (Fig. 4C) due to their differing average intensities. The boundaries of the GPi and GPe fit with predicted atlas boundaries and MER data. Standard T1 images (Fig. 4A) showed little contrast between the GPi, GPe, or the PLIC, but there was visible differentiation of pallidum and striatum with this sequence. T2-w FLAIR performed better than standard T1 (Fig. 4B), showing hypointensity around pallidum relative to striatum and the PLIC, but had less correspon-dence with atlas data than was seen with FGATIR. T2-w FLAIR failed to distinguish GPi and GPe and seem to overpredict the extent of pallidum medially and laterally (versus atlas predicted boundaries).
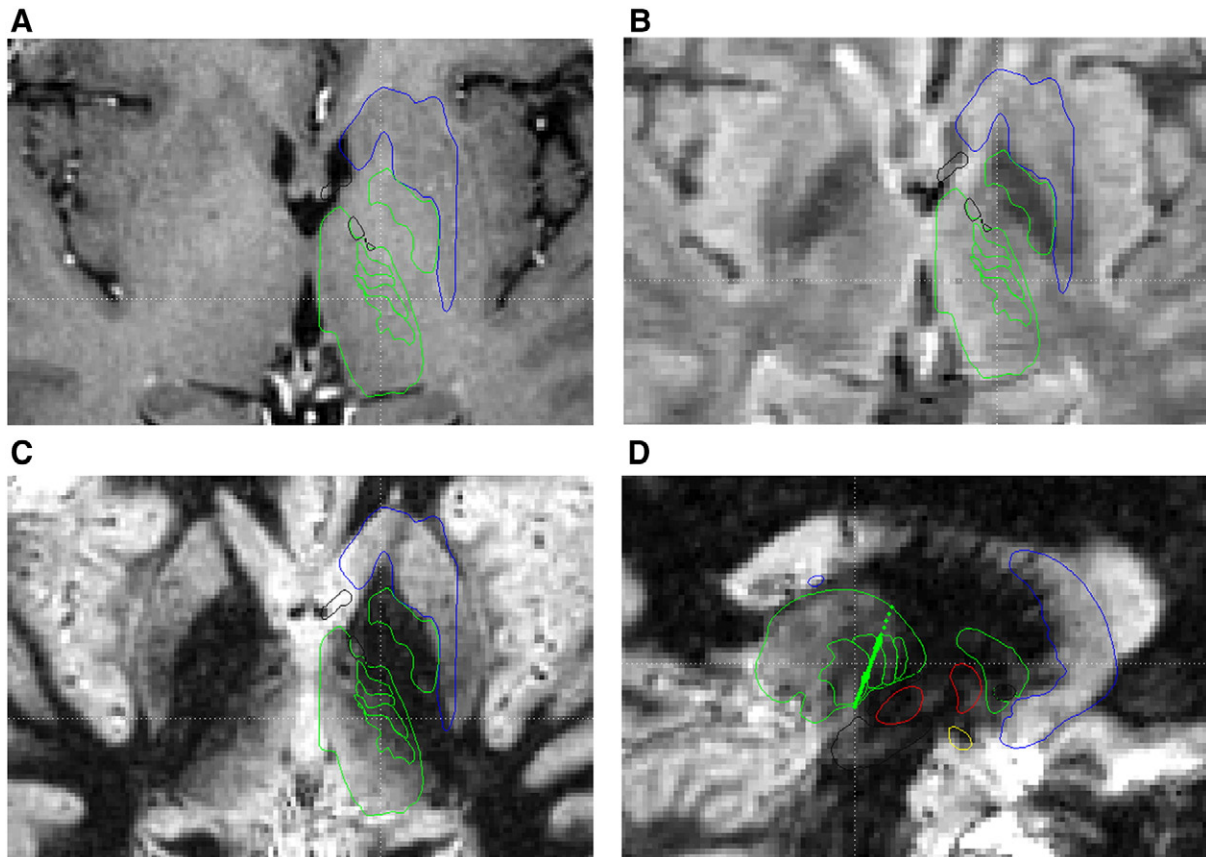

Fig. 3. Subcortical images from a thalamic Vim DBS patient (pre-surgery) showing axial slices (with deformable atlas overlay) on the (A) T1-w 3D MP-RAGE, (B) T2-w 3D FLAIR, (C) T1-w FGATIR, and a sagittal slice through the (D) T1-w FGATIR with MER maps overlaid (represented by the colored dots). The green contours within the thalamus represent the: (from anterior to poster) ventralis oralis anterior (Voa), ventralis oralis posterior (Vop), ventralis intermedius (Vim), and ventralis caudalis (Vc) nuclei of the thalamus. In panel D, the dot colors represent cells found for thalamus (green). Squares represent regions at which cellular response was seen during either passive movement or sensory stimulation of the patient.
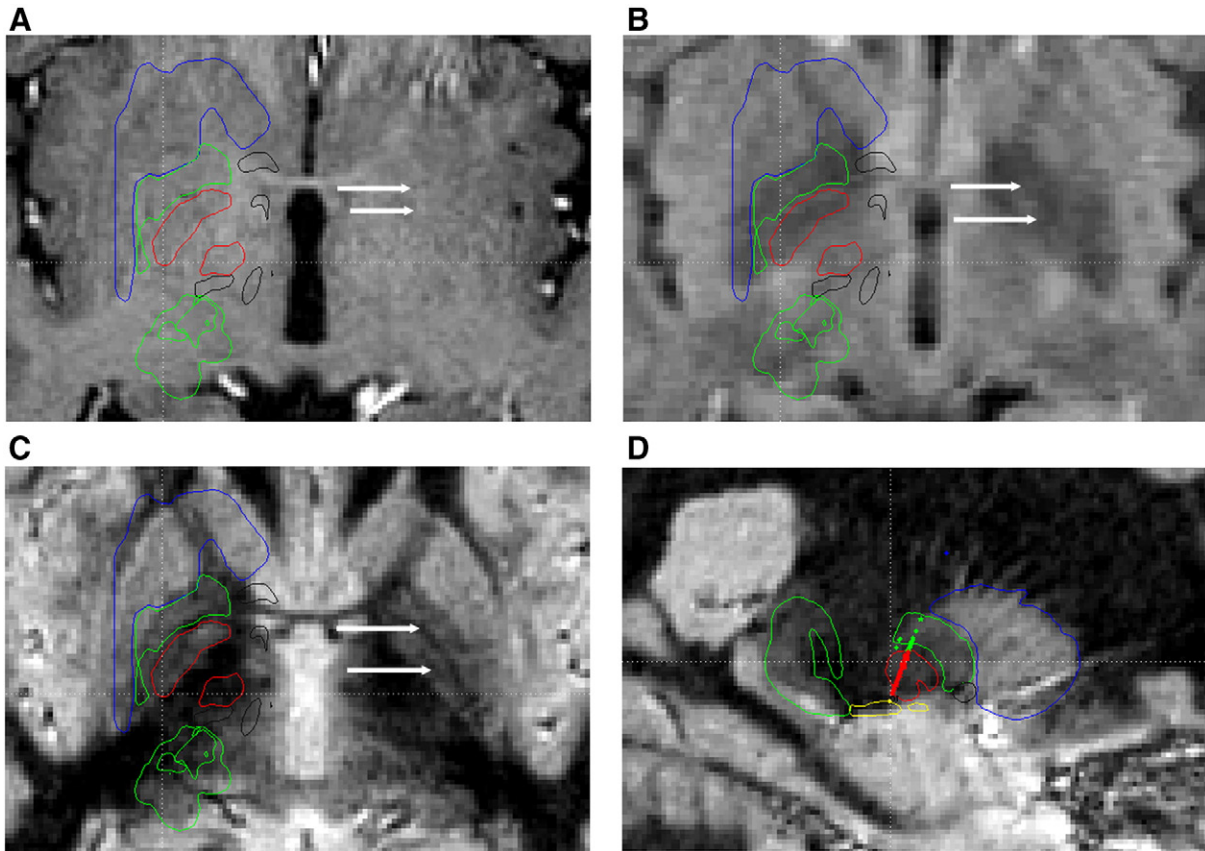
Fig. 4. Subcortical images from a GPi DBS patient (pre-surgery) showing axial slices (with deformable atlas overlay) on the (A) T1-w 3D MP-RAGE, (B) T2-w 3D FLAIR, (C) T1-w FGATIR, and a sagittal slice through the (D) T1-w FGATIR with MER maps overlaid (represented by the colored dots). The white arrows represent the location of the lamina between GPi/GPe and the lamina within GPi. In panel D, the dot colors represent cells found in GPi (red), GPe (green), striatum (blue), and optic tract (yellow).

Quantitative analysis

Fig. 5 summarizes the CRs and CNRs calculated for these three pilot MRI scans with respect to the DBS targets. In all cases the CNR and CR were higher when using the FGATIR scan than with either T1-w or T2-w FLAIR imaging, with the FGATIR showing the highest level of contrast across the regions analyzed.

Discussion

The DBS surgical procedure is focused primarily on obtaining accurate electrode placement. Imaging has played a central role in making this a reality. Progress in imaging – the stereotome, CT scans, and MRI – have all advanced DBS by making target localization more precise. Both T1 and T2 weighted scans have been employed in this regard. T1 weighted imaging has been a widely used scanning procedure for stereotactic surgery and radiosurgery due to its ability to produce thin slice, high resolution acquisitions within relatively short time periods. In our experience, T2 weighted MRI has been the primary high contrast imaging modality employed in DBS targeting for other groups due to its ability to visualize subcortical structures with high metal concentration. However the resolution and slice thickness have proven suboptimal. The FGATIR sequence in this pilot study offers significant advantages over both standard T1-w and T2-w FLAIR imaging for the three main targets utilized for DBS in movement disorders.

Previous efforts by others to image the basal ganglia by T2 weighted imaging have yielded mixed results. Good in-plane visualization of the STN with T2-w scan sequences has been reported by multiple groups (Dormont et al., 2004; Kitajima et al., 2008; Slavin et al., 2006). Slavin and colleagues were able to identify the

hypointense STN at 3T on relatively thin (1.5 mm) slice T2-w images. This required multiple planes of acquisitions for high resolution localization with a scanning time of approximately 30 min as compared to just over 11 min with the FGATIR. Other studies have tackled the problem of T2 localization of the STN and concluded that the hypointensity usually taken to represent STN sometimes represents solely the medial portion of the STN (Dormont et al., 2004). T2 visualization of the STN is also made problematic by interpatient variation in iron deposition in the basal ganglia that causes the T2 contrast to be visible to the human eye (Dormont et al., 2004). For these reasons T2-weighted imaging alone does not provide sufficient or consistent contrast of certain key structures of the basal ganglia. This lack has been compounded through the thick slice acquisition methods used in 2D FSE, with slices of 2 mm or more being typical.

T1 weighted imaging has also proved awkward at visualizing structures at the brain's center. Standard T1-weighted imaging has been used to acquire thin slice images (using MP-RAGE or turbo field echo sequences) although with seemingly less contrast than with thicker-slice T2-weighted images. Recent results indicate that T1-weighting itself should provide significant contrast compared to T2-weighted imaging for the thalamus, thalamic subnuclei (Deoni et al., 2005; Mercado et al., 2006), and the STN (Deoni et al., 2005). Deoni et al. (2005) acquired an ultra-high resolution T1 map that was able to delineate thalamic regions but at acquisition times that were far too long (several hours) for easy clinical application. In a paper by Reich et al. (2000), the authors described a 2D fast spin echo inversion recovery (FSE-IR) sequence. While they were able to identify the GPi, the resolution was low and the slice thickness was relatively thick (2 mm) due to the use of a 2D FSE based inversion recovery sequence. This sequence required 27.5 min of scanning time in order to allow for multiple planes of acquisition and sufficient averaging. The work of
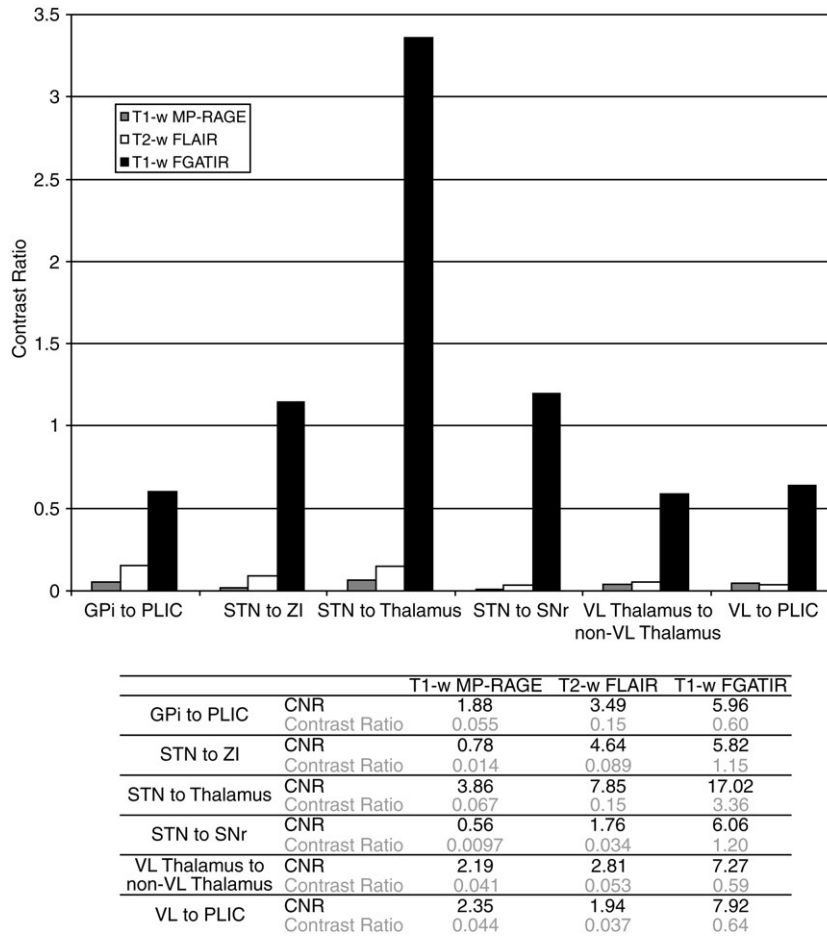
		T1-w MP-RAGE	T2-w FLAIR	T1-w FGATIR
GPi to PLIC	CNR	1.88	3.49	5.96
	Contrast Ratio	0.055	0.15	0.60
STN to ZI	CNR	0.78	4.64	5.82
	Contrast Ratio	0.014	0.089	1.15
STN to Thalamus	CNR	3.86	7.85	17.02
	Contrast Ratio	0.067	0.15	3.36
STN to SNr	CNR	0.56	1.76	6.06
	Contrast Ratio	0.0097	0.034	1.20
VL Thalamus to non-VL Thalamus	CNR	2.19	2.81	7.27
	Contrast Ratio	0.041	0.053	0.59
VL to PLIC	CNR	2.35	1.94	7.92
	Contrast Ratio	0.044	0.037	0.64

Fig. 5. Contrast ratios (CR) for GPi/PLIC, STN/ZI, STN/Thalamus, STN/SNr, VL Thalamus/non-VL Thalamus, and VL Thalamus/PLIC. The contrast ratio of the FGATIR sequence is higher than seen with either the T1-w or the T2-w FLAIR scans. Numerical values for both CR and CNR are listed in the bottom portion.

these groups shows the potential for T1 as a vehicle for imaging the basal ganglia, but a high resolution, high contrast, thin slice scan in clinically feasible scan time has yet to be demonstrated.

Our work focused on optimization of the T1 contrast mechanism. The FGATIR was based on a standard T1-w MP-RAGE sequence but incorporated the idea of nullification found in FLAIR and short tau inversion recovery (STIR): nullification of CSF signal (as in FLAIR) and nullifying the signal from fat (as in STIR). This allowed white matter signal nullification and an image that, in brain parenchyma, resulted from a gray matter only signal. Though the concept of nullification is not completely novel, the FGATIR's optimization of the full inversion pre-pulse prior (to nullify the white matter signal) to a fast 3D acquisition sequence may produce fast high resolution and thin slice scans as compared to either standard 2D FSE or 2D FSE-IR based sequences.

The FGATIR's preferential nullification of white matter signal allows for excellent delineation of grey matter structures that are surrounded by highly myelinated areas, such as structures in the basal ganglia. For example, the thalamus is bounded laterally by the internal capsule, superiorly by the corona radiata, and inferiorly by the zona incerta and afferent brainstem and cerebellar tracts. The GPi is a grey matter structure bordered on its posterior and medial extent by the internal capsule and anteriorly by the heavily myelinated lamina between GPi and GPe. As can be seen from Figs. 1–5, the contrast ratio for the FGATIR sequence is in general higher than that seen by the other two acquired sequences.

Though the STN is well visualized on the FGATIR, the reasons for its visualization are less clear. The STN is a gray matter structure and appears hypointense on our scan sequence. This may represent a high degree of myelination relative to neighboring grey matter structures.

Similar contrast has been reported with STIR images (Kitajima et al., 2008). It is interesting to note that the VL thalamus is similarly darker than its surroundings on FGATIR. This may similarly suggest that the VL thalamus has more white matter connections than the non-VL thalamus.

The quantitative results from this pilot work are in line with our qualitative results (Fig. 5). The most dramatic CNR was found between STN and the thalamus on the FGATIR sequence (17.02. versus 7.85 on T2 FLAIR). While T2 images are currently considered to be the best clinical scan for the localization of STN by most other groups, the CNR between the STN and SNr was 1.76 for the T2-weighted FLAIR scan versus 6.06 on the FGATIR scan. The distinct boundary between STN and SNr has been the most useful boundary in localization of STN on the FGATIR.

It should be noted that since FLAIR and FGATIR contrast between STN and SNr is different, the STN may at first appear thinner on the FGATIR than on the FLAIR. This size difference may be more apparent than actual. Both the STN and SNr are hypointense on FLAIR images, creating an area of low contrast between STN and SNr (as seen in contrast measurements in Fig. 5), which can make it difficult to see the STN's inferior border. Referring to the sagittal slice (Fig. 2D) helps rectify this, revealing a hypointense region superior to SNr and inferior to ZI that corresponds well to the atlas predicted site and size of STN. The atlas also suggests better FGATIR correspondence to the STN outline than seen on T2 FLAIR. On FLAIR images, the STN (hypointense region within the red contour seen in Fig. 2B on the left hemisphere) is smaller than the atlas predicted region and only fills a small portion of the atlas contour for STN. On FGATIR images, STN (hypointense) seems to be of at least the same size as compared to T2 imaging and also appears to better match the size of the atlas predicted region in

the lateral extent. Figs. 2B and C show a red line (of equivalent length in both panels) on the right hemisphere (left side of image) that represents the superior to inferior extents of the STN for both FLAIR and FGATIR imaging. The hypointense region in both the FGATIR and FLAIR appears to be roughly the same size in the superior to inferior boundary.

While the boundary between ZI and STN is an important one to identify clearly, as it marks the STN's superior boundary, there can be seen heterogeneous intensities in the superior STN and inferior ZI region. The origin of these is unclear. From Fig. 2C, it can be seen that there is a thicker region of hypointensity just inferior to thalamus and superior to the STN which, on the atlas, maps onto ZI. This hypointensity fits well with the description of ZI as an axon-rich structure. Based on empirical data from T1 images and our MER mapping data, the hypointense region directly superior to SNr appears to map to STN. The origin of the hyperintense region found immediately superior to STN is unclear. Our atlas deformation technique consistently maps it to superior STN/inferior ZI, but the appropriate interpretation of the heterogeneity of the MR signal in this area is currently indeterminate. We plan to further evaluate the hyperintensity between ZI and STN in the FGATIR via an imaging/histological study of a fresh cadaver brain.

DBS imaging has generally fallen into two seemingly mutually exclusive categories: high resolution thin slice MRI and high contrast thick slice MRI. Many groups have focused on obtaining excellent contrast in plane at the expense of localization along the slice axis (Dormont et al., 2004; Kitajima et al., 2008; Reich et al., 2000; Slavin et al., 2006). Fig. 6 shows a reconstruction of the FGATIR scan at various axial slice distances: 1 mm (Figs. 6A,B), 2 mm (Fig. 6C), and 3 mm (Fig. 6D). The reconstructed views (coronal in Fig. 6) show worsening resolution as the simulated slice distance is increased. It is worth noting that despite the high contrast seen with 3 mm slices, they are too thick to be useful for direct targeting of STN or GPi as the boundaries in the reconstructed image can no longer be easily delineated (Fig. 6D). The ability of the FGATIR sequence to acquire thin slice high resolution images is crucial to its utility as a tool for imaging the basal ganglia.

The ability of the FGATIR sequence to acquire both thin and high contrast slices is a significant improvement over the current sequences of choice: the 2D FSE-IR or 2D FSE T2-w. Using these 2D sequences can limit slice thickness to a minimum of 2 mm due to hardware gradient specifications. With the FGATIR sequence the slice thickness is no longer hardware gradient limited. The scan is fully 3D and slice thickness is limited only by acquisition time and signal considerations. Another advantage of the FGATIR is that at 1 mm slice thickness it offers nearly isotropic voxels. This allows for multi-planar reconstruction (MPR) and true 3D manipulation. The anisotropic voxels from 2 mm (or thicker) slice thickness 2D scans offer poor resolution when subjected to these reconstructions (Fig. 6) and transformations.

Our pilot work demonstrates that the contrast between target and surrounding tissue on the FGATIR is superior to standard T1-w and T2-w FLAIR imaging. This combination of short scan time, high resolution, thin slices, and high contrast has not previously been reported. Future work will involve the analysis of the FGATIR across a larger number of patients to determine the level of detectability across our patient populations. Due to the flexibility of this scan technique, we may be able to take advantage of newer hardware such as multichannel phased array head coils in order to increase the SNR as well as implement higher resolution and even faster acquisitions (through parallel imaging). Our initial results on a Philips 3T Achieva MRI with SENSE indicate that submillimeter (0.75 mm) slice thicknesses may be acquired within 10 min using an 8-channel headcoil. It is also possible to implement this sequence on standard 1.5T machines, but it should be noted that (as with any other sequence) the parameters would have to be changed accordingly to produce similar contrast characteristics — the parameters listed in Table 1 have been optimized for 3T implementation.

The consequences of the FGATIR sequence for DBS may prove to be substantial. Our future work will examine the effect the FGATIR has on being able to directly visualize and target the structures of interest. Since only a few patient scans have thus far been evaluated we were unable to quantitatively determine whether the use of this imaging protocol reduces the number of MER passes. We did find qualitatively
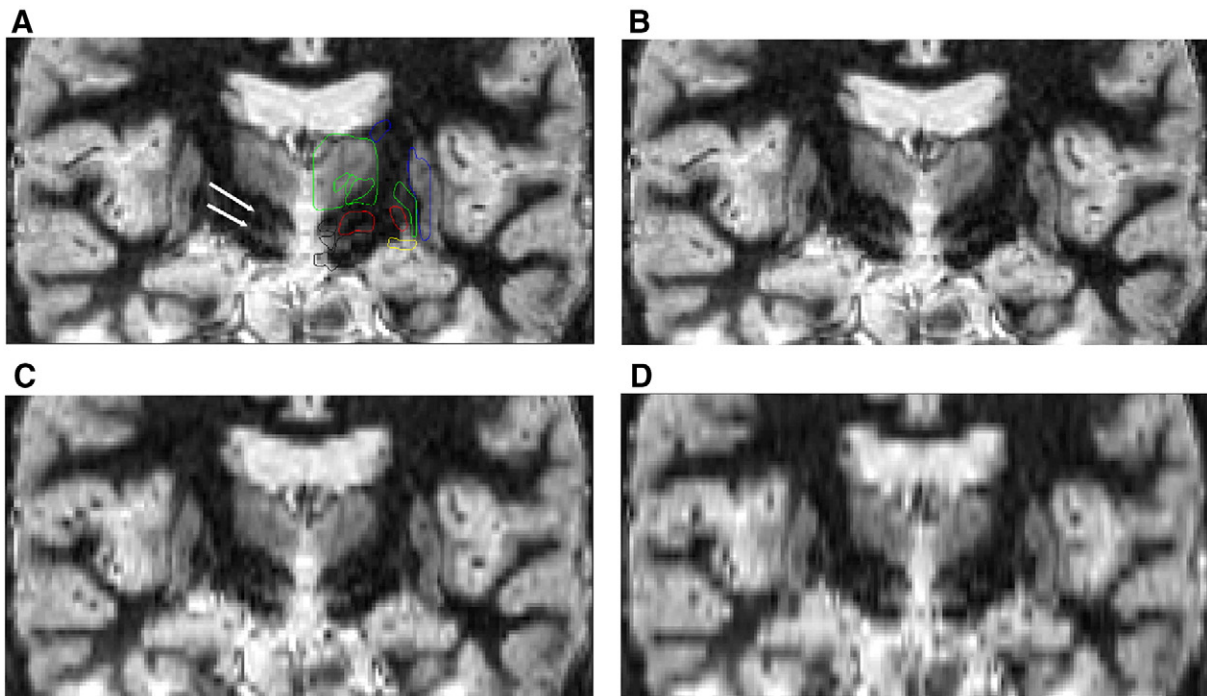

Fig. 6. Simulated FGATIR images at 1 mm (A,B), 2 mm (C), and 3 mm (D) slice spacing. The superior and inferior boundaries of STN are visible in (A) and (B) as shown by the white arrows in panel A, but are difficult to identify in (C) and (D).

that our operating room team was better able to recognize structures during preoperative targeting, increasing the ease of atlas deformation and ease of selection of the coordinates of the initial MER pass. We expect that the end result of this improved imaging method will be a reduction in operating room time via a reduction of MER passes, intraoperative testing, and potentially DBS lead relocation due to suboptimal initial implantation. Length of time spent in surgery is a well known correlate to surgical complication rates and reducing the time the patient spends on the OR table would be expected to significantly decrease morbidity. For example, the number of MER passes has been correlated with the risk of intraoperative hemorrhage (Gorgulho et al., 2005).

We do expect that better direct imaging will decrease the amount of MER required to arrive at target and will examine this question more closely. We also expect improved imaging of the basal ganglia to allow us to better define the degree of interpatient variability in basal ganglia extent and structure. Most atlases are based on the careful dissection of a small number of brains. The FGATIR may allow us to substantially expand this data set, thereby improving our ability to understand and adapt to the anatomical variations underlying individual patients' disease.

Conflict of interest
The authors declare that there is no conflict of interest.

References

Amirnovin, R., Williams, Z.M., Cosgrove, G.R., Eskandar, E.N., 2006. Experience with microelectrode guided subthalamic nucleus deep brain stimulation. Neurosurgery 58, ONS96–ONS102 discussion ONS196-102.
Bootin, M.L., 2006. Deep brain stimulation: overview and update. J. Clin. Monit. Comput. 20, 341–346.
Chakravarty, M.M., Sadikot, A.F., Germann, J., Bertrand, G., Collins, D.L., 2008. Towards a validation of atlas warping techniques. Med. Image Anal. 12 (6), 713–726.
Chen, S.Y., Lee, C.C., Lin, S.H., Hsin, Y.L., Lee, T.W., Yen, P.S., Chou, Y.C., Lee, C.W., Annie Hsieh, W., Su, C.F., Lin, S.Z., 2006. Microelectrode recording can be a good adjunct in magnetic resonance image-directed subthalamic nucleus deep brain stimulation for parkinsonism. Surg. Neurol. 65, 253–260 discussion 260–261.
Cosyns, P., Gabriels, L., Nuttin, B., 2003. Deep brain stimulation in treatment refractory obsessive compulsive disorder. Verh. K. Acad. Geneeskd. Belg. 65, 385–399 discussion 399–400.
DBSPDSG, 2001. Deep-brain stimulation of the subthalamic nucleus or the pars interna of the globus pallidus in Parkinson's disease. N. Engl. J. Med. 345, 956–963.
Deoni, S.C., Josseau, M.J., Rutt, B.K., Peters, T.M., 2005. Visualization of thalamic nuclei on high resolution, multi-averaged T1 and T2 maps acquired at 1.5 T. Hum. Brain Mapp. 25 (3), 353–359.
Dormont, D., Ricciardi, K.G., Tande, D., Parain, K., Menuel, C., Galanaud, D., Navarro, S., Cornu, P., Agid, Y., Yelnik, J., 2004. Is the subthalamic nucleus hypointense on T2-weighted images? A correlation study using MR imaging and stereotactic atlas data. AJNR Am. J. Neuroradiol. 25, 1516–1523.
Duffner, F., Schiffbauer, H., Breit, S., Friese, S., Freudenstein, D., 2002. Relevance of image fusion for target point determination in functional neurosurgery. Acta Neurochir. (Wien) 144, 445–451.
Gorgulho, A., De Salles, A.A., Frighetto, L., Behnke, E., 2005. Incidence of hemorrhage associated with electrophysiological studies performed using macroelectrodes and microelectrodes in functional neurosurgery. J. Neurosurg. 102, 888–896.
Greenberg, B.D., Malone, D.A., Friehs, G.M., Rezai, A.R., Kubu, C.S., Malloy, P.F., Salloway, S.P., Okun, M.S., Goodman, W.K., Rasmussen, S.A., 2006. Three-year outcomes in deep brain stimulation for highly resistant obsessive–compulsive disorder. Neuropsychopharmacology 31, 2384–2393.
Hung, S.W., Hamani, C., Lozano, A.M., Poon, Y.Y., Piboolnurak, P., Miyasaki, J.M., Lang, A.E., Dostrovsky, J.O., Hutchison, W.D., Moro, E., 2007. Long-term outcome of bilateral pallidal deep brain stimulation for primary cervical dystonia. Neurology 68, 457–459.
Kitajima, M., Korogi, Y., Kakeda, S., Moriya, J., Ohnari, N., Sato, T., Hayashida, Y., Hirai, T., Okuda, T., Yamashita, Y., 2008. Human subthalamic nucleus: evaluation with high-resolution MR imaging at 3.0 T. Neuroradiology 50 (8), 675–681.
Kumar, R., Lozano, A.M., Sime, E., Lang, A.E., 2003. Long-term follow-up of thalamic deep brain stimulation for essential and parkinsonian tremor. Neurology 61, 1601–1604.
Lee, M.W., De Salles, A.A., Frighetto, L., Torres, R., Behnke, E., Bronstein, J.M., 2005. Deep brain stimulation in intraoperative MRI environment — comparison of imaging techniques and electrode fixation methods. Minim. Invasive Neurosurg. 48, 1–6.
Lozano, A.M., Mayberg, H.S., Giacobbe, P., Hamani, C., Craddock, R.C., Kennedy, S.H., 2008. Subcallosal cingulate gyrus deep brain stimulation for treatment-resistant depression. Biol. Psychiatry 64, 461–467.
Mercado, R., Mandat, T., Moore, G.R., Li, D., MacKay, A., Honey, C.R., 2006. Three-tesla magnetic resonance imaging of the ventrolateral thalamus: a correlative anatomical description. J. Neurosurg. 105 (2), 279–283.
Nuttin, B.J., Gabriels, L., van Kuyck, K., Cosyns, P., 2003. Electrical stimulation of the anterior limbs of the internal capsules in patients with severe obsessive–compulsive disorder: anecdotal reports. Neurosurg. Clin. N. Am. 14, 267–274.
Okun, M.S., Fernandez, H.H., Pedraza, O., Misra, M., Lyons, K.E., Pahwa, R., Tarsy, D., Scollins, L., Corapi, K., Friehs, G.M., Grace, J., Romrell, J., Foote, K.D., 2004. Development and initial validation of a screening tool for Parkinson disease surgical candidates. Neurology 63, 161–163.
Okun, M.S., Mann, G., Foote, K.D., Shapira, N.A., Bowers, D., Springer, U., Knight, W., Martin, P., Goodman, W.K., 2007. Deep brain stimulation in the internal capsule and nucleus accumbens region: responses observed during active and sham programming. J. Neurol. Neurosurg. Psychiatry 78, 310–314.
Pahwa, R., Lyons, K.E., Wilkinson, S.B., Simpson Jr., R.K., Ondo, W.G., Tarsy, D., Norregaard, T., Hubble, J.P., Smith, D.A., Hauser, R.A., Jankovic, J., 2006. Long-term evaluation of deep brain stimulation of the thalamus. J. Neurosurg. 104, 506–512.
Pinsker, M.O., Volkmann, J., Falk, D., Herzog, J., Alfke, K., Steigerwald, F., Deuschl, G., Mehdorn, M., 2008. Electrode implantation for deep brain stimulation in dystonia: a fast spin-echo inversion-recovery sequence technique for direct stereotactic targeting of the GPI. Zentralbl. Neurochir. 69 (2), 71–75.
Rampini, P.M., Locatelli, M., Alimehmeti, R., Tamma, F., Caputo, E., Priori, A., Pesenti, A., Rohr, M., Egidi, M., 2003. Multiple sequential image-fusion and direct MRI localisation of the subthalamic nucleus for deep brain stimulation. J. Neurosurg. Sci. 47, 33–39.
Reich, C.A., Hudgins, P.A., Sheppard, S.K., Starr, P.A., Bakay, R.A., 2000. A high-resolution fast spin-echo inversion-recovery sequence for preoperative localization of the internal globus pallidus. AJNR Am. J. Neuroradiol. 21, 928–931.
Schaltenbrand, G., Bailey, P., 1959. Einführung in die stereotaktischen Operationen, mit einem Atlas des menschlichen Gehirns. Introduction to Stereotaxis, With an Atlas of the Human Brain. Thieme, Stuttgart.
Slavin, K.V., Thulborn, K.R., Wess, C., Nersesyan, H., 2006. Direct visualization of the human subthalamic nucleus with 3T MR imaging. AJNR Am. J. Neuroradiol. 27, 80–84.
Temel, Y., Visser-Vandewalle, V., 2004. Surgery in Tourette syndrome. Mov. Disord. 19, 3–14.
Wider, C., Pollo, C., Bloch, J., Burkhard, P.R., Vingerhoets, F.J., 2008. Long-term outcome of 50 consecutive Parkinson's disease patients treated with subthalamic deep brain stimulation. Parkinsonism Relat. Disord. 14, 114–119.
Zorzi, G., Marras, C., Nardocci, N., Franzini, A., Chiapparini, L., Maccagnano, E., Angelini, L., Caldiroli, D., Broggi, G., 2005. Stimulation of the globus pallidus internus for childhood-onset dystonia. Mov. Disord. 20, 1194–1200.